

A Bayesian Monte Carlo assessment of orbital stability in the late stages of planetary system formation

Jassyr Salas,^{1*} Frank Bautista,² and Germán Chaparro³

¹Universidad del Atlántico, Barranquilla, Colombia

²Universidad Nacional de Colombia, Bogotá, Colombia

³FACom, Instituto de Física - FCEN, Universidad de Antioquia, Calle 70 No. 52-21, Medellín, Colombia.

Accepted XXX. Received YYY; in original form ZZZ

ABSTRACT

The final orbital configuration of a planetary system is shaped by both its early star-disk environment and late-stage gravitational interactions. Assessing the relative importance of each of these factors is not straightforward due to the observed diversity of planetary systems compounded by observational biases. Our goal is to understand how a planetary system may change when planetesimal accretion and planet migrations stop and secular gravitational effects take over. Our approach starts with a novel classification of planetary systems based on their orbital architecture, validated using Approximate Bayesian Computation methods. We apply this scheme to observed planetary systems and also to ~ 400 synthetic systems hosting ~ 5000 planets, synthesized from a Monte Carlo planet population model. Our classification scheme robustly yields four system classes according to their planet masses and semi-major axes, for both observed and synthetic systems. We then estimate the orbital distribution density of each of the synthetic systems before and after dynamically evolving for 0.1-1 Myr using a gravitational+collisional N -body code. Using the Kullback-Leibler divergence to statistically measure orbital configuration changes, we find that $\lesssim 10\%$ of synthetic planetary systems experience such changes. We also find that this fraction belongs to a class of systems for which their center of mass is very close to their host star. Although changes in the orbital configuration of planetary systems may not be very common, they are more likely to happen in systems with close-in, massive planets, with F- and G-type host-stars and stellar metallicities $[\text{Fe}/\text{H}] > 0.2$.

Key words: methods: statistical – catalogues – software: simulations – planets and satellites: dynamical evolution and stability – planets and satellites: formation – planet–star interactions

1 INTRODUCTION

Exoplanet catalogs have grown by significant leaps as new instruments have come operational (Bashi et al. 2018; Guerrero et al. 2021) and the boundaries of the parameter space that defines exoplanetary system configurations has been constantly redefined ever since exoplanets were first detected (Udry & Santos 2007). On the other hand, conclusions based on theories and numerical simulations developed for the early stages and the formation of the Solar System, explain how the dissipation of gas leads to instabilities that result in migrations and the formation of rocky planets Liu et al. (2022), however, they are often difficult to apply to the formation history of other planetary systems (Raymond et al. 2009; Woo et al. 2022). Additionally, exoplanet observations have biases that favor the detection of short-period planets. Therefore, deducing the physical conditions in which planetary systems are born based only on current observations is not straightforward.

However, despite the difficulty in overcoming detection biases, in recent years the number of detected exoplanetary systems appears to represent a partial but robust sampling of the parameter space for the

physical conditions in which these systems form (Bryson et al. 2021; Bashi & Zucker 2021). Modern statistical methods can then be used to compare synthetic and observational results in order to make a meaningful taxonomy of planetary systems (Chaparro Molano et al. 2018; Rogers & Owen 2021).

Deterministic models of the formation of planetary systems yield planetary system configurations that are highly sensitive to context-dependent effects such as dynamical instabilities and migration (Ida & Lin 2004; Schlecker, M. et al. 2021). Therefore it is important to elucidate whether secular gravitational interactions play a role in the final configuration of a planetary system.

Here we present a study of planet formation in its final stages, when planetesimal accretion is mostly finished and protoplanets become gravitationally isolated planets Beaugé & Aarseth (1990); Mordasini et al. (2009a). This last stage is ruled by gravitational interactions between planets and planetesimals that tend to perturb their orbits when close encounters and collisions occur, until a final configuration of planets in differentiated stable orbits is achieved (Andryushin & Popov 2021). This analysis can be done through computer simulations of synthetic planetary populations. Understanding this last phase is also of particular interest because the last impact record Alexander & Agnor (1998) and the possible formation of satellites

* E-mail: sjassyr@mail.uniatlantico.edu.co

are thought to emerge here (Alvarado-Montes et al. 2017; Sucerquia et al. 2019).

Therefore our main objective is to analyze the effect that these gravitational interactions have on the development and evolution of exoplanet populations, using a model of collisions between newly-accreted planets that depend on the impact energy between them. We propose a statistical framework to compare the initial and final configurations with a reconstruction of the posterior probability, which could help guide future exoplanet surveys.

We also implement a novel classification scheme for observational and synthetic planetary systems, which improves upon previous machine learning-based algorithms Naderi et al. (2019) in terms of adaptability and the fact that we focus on system-wide orbital characteristics. This is also of great help in understanding how the systems change after considering the gravitational interactions and evolution of exoplanets.

This work is structured as follows: firstly, in section 2 we go through the observational and synthetic data and describe our classification scheme. Then in Section 3 we describe the collisional N -body model used in the simulations and the statistical methods used for assessing system-wide orbital changes. In Section 4 we discuss our results of the simulations, contrasting with the [The Extrasolar Planets Encyclopaedia \(1995\)](#) database, and finish with our conclusions in Section 5.

2 PLANETARY SYSTEM DATA

Our main focus in this work is to understand how the final orbital configuration of exoplanetary systems depends on stellar parameters and/or on secular gravitational effects. However, we first need to understand why observed planetary systems populations may differ from planetary population synthesis results. To this end, we use Unsupervised Learning and Approximate Bayesian Computation methods in order to compare observational and synthetic data, thus getting a grasp on the possible impact of observational biases.

2.1 Observational data

Observations of exoplanetary systems give us a wide variety of data to benchmark planet formation models against. One of the most complete and public exoplanet databases is [The Extrasolar Planets Encyclopaedia \(1995\)](#) (Schneider et al. 2011), founded by the *Observatoire de Paris*. The catalogue relates the physical parameters of exoplanets and the physical information of the host stars. In this database, substellar bodies with masses between $1 \times 10^{-5} (M_{\text{Jup}})$ to $8 \times 10^1 (M_{\text{Jup}})$ are taken to be planets.

2.2 Synthetic data

Planet population synthesis models describe how the physical evolution of protoplanetary disks results in planetary systems with properties that agree with observations. Mordasini et al. (2009a,b); Alibert et al. (2011) and Miguel et al. (2011) inasmuch observed planetary systems that can be reproduced using these formulations. Current models strive to reach self-consistent, generative recipes for planetary formation with the use of Monte Carlo techniques (Benz et al. 2014), but observational biases create a gap between theoretical predictions and observations.

In order to create a synthetic planetary data set we follow the Monte Carlo planet formation recipe of Miguel et al. (2011); Chapparro Molano et al. (2018). Here, planets grow in individual systems

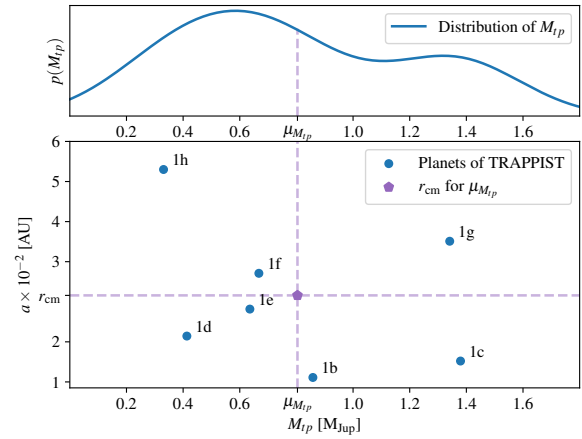


Figure 1. Kernel density estimation of the planet mass distribution $\mu_{M_{\text{Jup}}}$ (above) and semi-major axis vs. planet mass (below) for the TRAPPIST-1 system. The dashed line corresponds to the first moment of the planet mass wrt the semi-major axis, or *center of mass* r_{cm} .

Table 1. Initial conditions for our planet population synthesis model. The probability distribution functions are constructed from observations of exoplanetary systems (Miguel et al. 2011).

Stellar mass $M_{\star} [M_{\odot}]$	$\log(\mathcal{U}(a_{M_{\star}}, b_{M_{\star}}))$	$a_{M_{\star}} \sim 0.7,$ $b_{M_{\star}} \sim 1.4,$
Mass of the disk $M_d [M_{\odot}]$	$\log(\mathcal{N}(\mu_{M_d}, \sigma_{M_d}))$	$\mu_{M_d} = -2.05,$ $\sigma_{M_d} = 0.85.$
Radial extent a [AU]	$\log(\mathcal{N}(\mu_a, \sigma_a))$	$\mu_a = 3.8,$ $\sigma_a = 0.81.$
Stellar metallicity [Fe/H]	$\mathcal{N}(\mu, \sigma)$	$\mu = -0.02,$ $\sigma = 0.22.$
Time of gas dissipation τ_g [y]	$\log(\mathcal{U}(a_{\tau_g}, b_{\tau_g}))$	$a_{\tau_g} \sim 10^6,$ $b_{\tau_g} \sim 10^7.$

following an oligarchic growth model of solid cores coupled with a core instability model for gas accretion along with Types I and II migration. The physical variables that we use as initial conditions for the simulations are summarized in Table 1, along with the probability distributions from which the initial conditions for individual simulations were drawn. These distributions, which effectively work as prior probability distributions are constructed from observations of exoplanetary systems (Miguel et al. 2011).

The results of these simulations are masses and semi-major axes for all planets formed in individual systems. From this we compute physical properties that describe each system which allows us to make a statistical comparison to observed exoplanetary systems.

We thus ran simulations yielding 1200 synthetic systems for which properties listed in Table 1 are known. It is noteworthy that according to these planet population synthesis simulations only about 20% of systems have giant planets.

2.3 Center-of-mass clustering of planetary systems

Seeking to improve upon existing exoplanetary system classification schemes, and wishing to assess the role of observational biases when comparing observations with planet population synthesis results, we built an unsupervised learning model based on the exoplanet mass distribution along the orbital plane of each system. Existing classification schemes are based on ad-hoc comparisons of exoplanetary

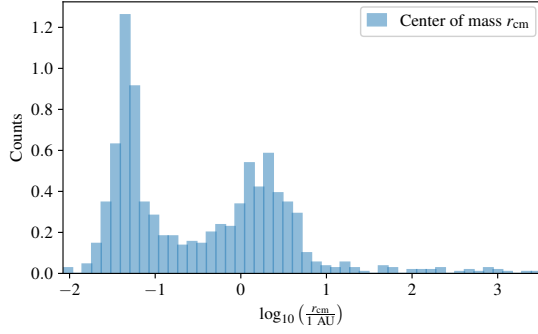


Figure 2. Histogram for the log-center of mass r_{cm} of observed planetary systems. We use the log due to the fact that the center of mass range spans many orders of magnitudes.

systems and mostly look at superficial similarities between planetary systems [Miguel et al. \(2011\)](#); [Benz et al. \(2014\)](#), and are understandably concerned with matching properties of observed and simulated systems in order to avoid the effects of observational biases. Our approach to classification of observed and synthetic planetary systems is based on Gaussian Mixture Models (GMM) which is an unsupervised learning technique that requires no previous labeling and allow for the discovery of patterns in data ([VanderPlas 2016](#)). For this we used the the `scikit-learn` package [Pedregosa et al. \(2011\)](#).

Our variable of interest for this classification scheme needed to be system-wide variable with information about where in the disk most of the planet mass is located. We therefore used the first moment of planet mass distribution with respect to the semi-major axis. We call this variable the *center of mass* radius r_{cm} . As an illustration of how this works, Figure 1 shows the total planetary mass distribution M_{tp} , for the TRAPPIST-1 system and its center of mass r_{cm} , according to the public data from [The Extrasolar Planets Encyclopaedia \(1995\)](#). We also developed our own model validation technique based on the principles of Approximate Bayesian Computation (ABC).

We will refer to this classification scheme again in Section 4 to study the conditions in which planetary systems may shift clusters when considering gravitational interactions between planets.

2.3.1 Observational data classification

Figure 2 shows the distribution of the log-center of mass $\log r_{\text{cm}}$ for observed exoplanetary systems. There is a region with a bi-modal behaviour between $10^{-2} \text{ AU} < r_{\text{cm}} < 10 \text{ AU}$: the first peak corresponding to systems with hot Jupiters, whereas the second peak corresponds to systems more alike to our own Solar System. Additionally, there is an uniformly distributed region at $r_{\text{cm}} > 10$, corresponding to systems with planets which are located far away from their host star. In order to move beyond this superficial classification, we built an unsupervised learning classification scheme based on GMM.

Since GMMs allow as many Gaussian clusters as there are data points, overfitting is a possibility. However it can be avoided with the use of *information criteria* based on Occam’s razor, which penalize models that require too many clusters or in general too many fitting parameters ([Claeskens & Hjort 2008](#)). The most popular and versatile estimators are the *Akaike information criterion - AIC* proposed by [Akaike \(1974\)](#), and the *Bayesian information criterion - BIC* defined by [Schwarz \(1978\)](#).

We calculate these criteria for models with $k = 1, 2, 3, 4, \dots, 20$ clusters. The minimum result in the values of AIC and BIC indicates

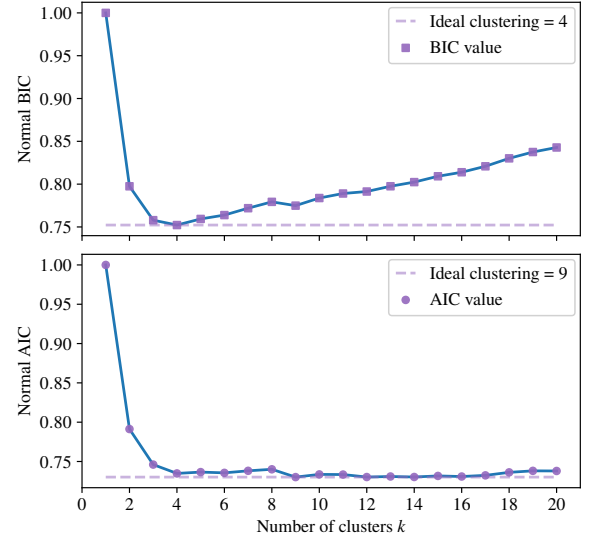


Figure 3. Normalized BIC and AIC values vs. number of GMM clusters k for center-of-mass clustering of observed exoplanetary systems.

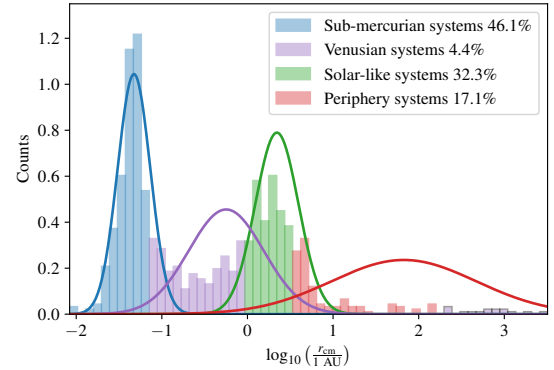


Figure 4. Gaussian Mixture Model with $k = 4$ clusters to classify observed exoplanetary systems according to their log center of mass.

the optimal mixture model. Figure 3 shows normalized values of AIC and BIC for log-center of mass clustering. The lowest BIC value is for a model with $k = 4$ clusters, and the lowest AIC value is for a $k = 9$ clusters. Thus, the BIC recommends a simpler model, which is preferred because BIC penalizes model complexity more heavily, as it accounts for the number of fitting parameters, while the AIC does not. Figure 4 shows the Gaussian Mixture Model with $k = 4$ clusters applied to the observed center of mass r_{cm} .

For easy reference, we named clusters by matching their mean center of mass with objects in the the Solar System orbiting at similar distances as follows: *Sub-Mercurian* ($0.01 \text{ AU} \leq r_{\text{cm}} < 0.1 \text{ AU}$) are systems that have a center of mass close to their host star, *Venusian* ($0.1 \text{ AU} \leq r_{\text{cm}} < 1 \text{ AU}$) are systems with a center of mass comparable to the approximate distance from Venus or the Earth to the Sun, *Solar-like* ($1 \text{ AU} \leq r_{\text{cm}} < 10 \text{ AU}$) are planetary systems with their center of mass located at a distance similar to that of Jupiter, which holds most of the planetary mass in our own Solar System, and *Peripheral* ($r_{\text{cm}} > 10 \text{ AU}$), systems whose center of mass is located beyond the regions where we find planets in our own Solar System.

2.3.2 Approximate Bayesian Computation validation

The classification scheme presented above is based upon a frequentist approach that does not consider the measurement uncertainties (Exoplanet Exploration Program, NASA 2010). In our case, the main sources of uncertainty is the planet mass and semi-major axis. Therefore, inspired by Approximate Bayesian Computation (ABC) we created a Monte Carlo validation scheme based on evaluating the robustness of the classification when checked against measurement errors. The approach is summarized as follows.

For each system we draw values of r_{cm} from the posterior distribution generated from the center of mass estimation, taking the prior distributions for the planet mass and semi-major axis as Gaussians with mean and variance from the reported measurement and corresponding error. We then check whether for 1000 draws from the r_{cm} posterior of each system, the posterior distribution of the clustering model predicts a different cluster from the original. Since we do not update the posterior distribution of the clustering model this validation scheme belongs to the ABC family of algorithms. If the posterior prediction re-classifies a system (with respect to the original classification) for more than 5% of the draws, we consider this an *in-between* system. Our validation scheme yields that less than 2% of observed exoplanetary systems are *in-betweeners*, which shows that our GMM-based classification scheme for r_{cm} across systems is indeed robust.

2.3.3 Synthetic data classification

In order to better understand how observational biases may affect classification schemes, we applied the same classification scheme shown above to the $\log-r_{\text{cm}}$ of synthetic systems generated from the planetary population synthesis model of Miguel et al. (2011); Chaparro Molano et al. (2018), described in Section 2.2. The center of mass histogram in Figure 5 shows a uniform distribution of systems with center of mass between 0.1 AU and 1.5 AU, an approximately bi-modal distribution with a first peak near 5 AU and a second peak near 10 AU, and very few systems with centers of mass much greater than this value. This is because observed planetary systems with large centers of mass very likely have additional, yet unobserved planets close to their star, which would bring the value of r_{cm} down after detection. A comparison between the frequency of Solar-like systems relative to Sub-Mercurian in observational (Figure 4) and synthetic (Figure 5) data shows that current observations may be missing a factor of about 20x Solar-like exoplanetary systems (e.g. with centers of mass near 1-6 AU), and an additional population of systems with centers of mass near 10 AU. A significant sample of these populations is still beyond our current detection capabilities. Figure 6 shows the BIC and AIC for the GMM-based classification of planetary systems which yields $k = 4$ as the most reasonable number of clusters, shown in Figure 7. The classification schemes for observational and synthetic data roughly agree in that there are four populations of systems (i.e. Sub-Mercurian, Venusian, Solar-like, Peripheral according to our classification in Section 2.3.1), although our simulations show that the three clusters closest to the star are higher in center of mass by about half an order of magnitude with respect to the observational clusters. Again, this is explained by observational biases that favor detection of systems with massive, close-in planets, where further detections of high-mass, located at distances $\gtrsim 1$ AU from their star are unlikely with our current technology.

On the other hand, observational data in Figure 4 shows a fraction

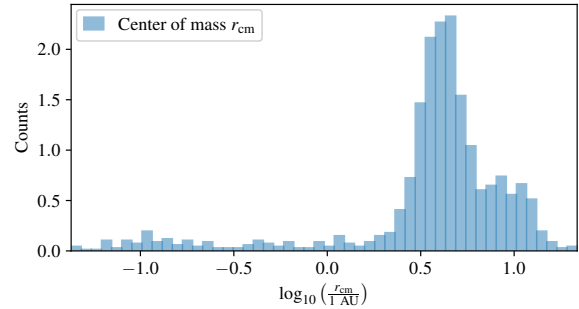


Figure 5. Log center of mass distribution for our synthetic planetary systems.

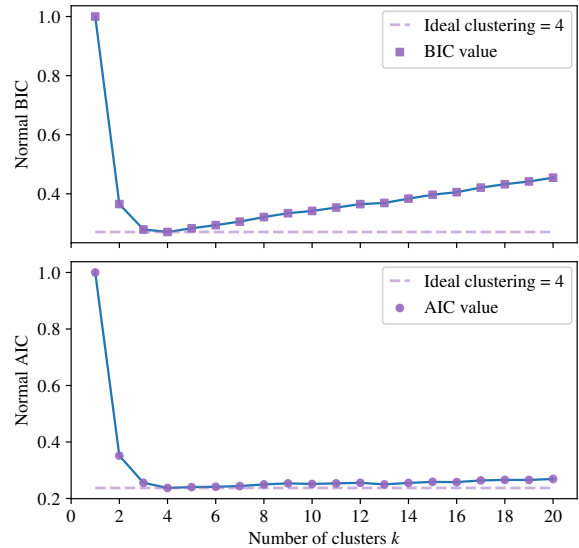


Figure 6. Normalized BIC and AIC values vs. number of GMM clusters k for center-of-mass clustering of synthetic planetary systems.

of systems with very large centers of mass ($r_{\text{cm}} \gg 10$ AU) that does not appear to be significant in synthetic systems (Figure 7). In the clustering of synthetic systems, the *peripheral* cluster is located between 6-20 AU, which is a significantly lower r_{cm} range than what observations seem to show. Systems in this range have been found by techniques such as gravitational lensing and direct imaging, which are biased toward extremely far-away planets (Kipping & Sandford 2016) with respect to other detection methods such as transit and radial velocity. Thus, these observed Periphery systems are likely extreme r_{cm} outliers which do not constitute a fair sample of all Periphery systems, most of which ($r_{\text{cm}} \sim 10$ AU) would currently be beyond our detection capabilities.

3 TOOLS FOR ASSESSING THE ROLE OF GRAVITATIONAL INTERACTIONS

In this section we discuss the gravitational-collision model and the statistical framework that will allow us to assess to what extent the final configuration of a synthetic planetary system is dependent on its secular evolution. To this end, we use an N -body numerical Leapfrog integrator of the equations of motion including gravitational interactions between all bodies. We also include a collision recipe based on the work of Alexander & Agnor (1998) which considers dynamic

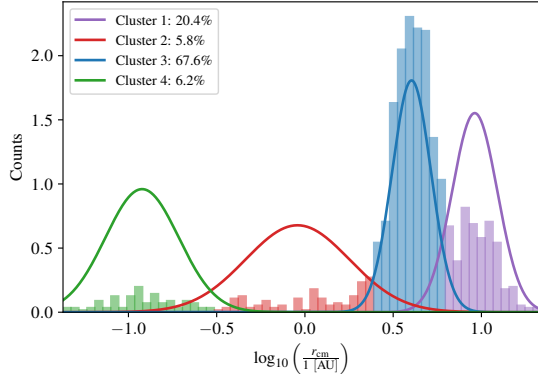


Figure 7. Gaussian Mixture Model with $k = 4$ clusters to classify synthetic planetary systems according to their log center of mass.

gravitational interactions between bodies with a variable time step for when collisions are in play. This formulation also includes recipes for rebound, fragmentation and mass exchange. This allows for an accurate tracking of planetary evolution.

3.1 Collision model

The outcome of a collision depends on the impact energy vis-a-vis and the resistance or hardness of the bodies. We first consider the collision of two planetesimals with total mass $M = m_1 + m_2$ (m_{12}) and with \mathbf{v}_1 and \mathbf{v}_2 as their respective velocities.

The possible outcomes of collisions can be: i. rebound, ii. rebound with mass exchange and iii. fragmentation; these lead to accretion when the planetesimals are dynamically unexcited, i.e., low impact velocity. On the other hand, high velocity impacts in dynamically excited populations (the present-day asteroid belt, debris disks, etc.) lead to a sequence of collisions that grind the bodies into very small particles [Armitage \(2018\)](#).

We define the total impact energy due to the relative motion of the bodies with respect to the center of mass as,

$$E = \frac{1}{2} \frac{m_1 m_2}{m_1 + m_2} V_r^2. \quad (1)$$

Here $\mathbf{V}_r = \mathbf{v}_2 - \mathbf{v}_1$. Since these collisions are expected to be mostly inelastic, a fraction η of the energy is dissipated as heat during the encounter. Thus, the energy E' after a collision would be,

$$E' = (1 - \eta)E. \quad (2)$$

Equation 1 yields the *rebound velocity*, i.e. the relative velocity between the two bodies immediately after the collision,

$$\mathbf{V}_{\text{reb}} = -c_i \mathbf{V}_r. \quad (3)$$

The quantity $c_i = \sqrt{1 - \eta}$ is the restitution coefficient, which can be considered as the ratio of the rebound and impact speeds.

3.1.1 Rebound

If the relative velocity is too low the collision will result in a rebound, i.e. both bodies collide and separate without exchange of mass. For this to occur the maximum stress on the surface of the body must be less than the impact strength of the planetesimal ([Greenberg et al.](#)

1978). In other words, the relative speed must satisfy the following condition,

$$V_r < V_c = \frac{2S}{c\rho_c}. \quad (4)$$

Here S is the impact strength defined as the capacity of a material to absorb energy and deform plastically without fracturing, c is the speed of sound and ρ_c is the characteristic density¹, which is of the order of the density of a typical rocky body in the Solar System. In this work we assume that for planets whose density ρ is lower than our assumed value (e.g. for gas giants) there is a characteristic impact radius at which the planet behaves as a solid body with density ρ_c .

The new velocities after the collision are then,

$$\mathbf{v}'_1 = \mathbf{V}_G - \left(\frac{m_2}{M}\right) \mathbf{V}_{\text{reb}}, \quad (5)$$

$$\mathbf{v}'_2 = \mathbf{V}_G + \left(\frac{m_1}{M}\right) \mathbf{V}_{\text{reb}}.$$

Here \mathbf{V}_G is the velocity of the center of mass of the two colliding bodies.

3.1.2 Rebound with mass exchange

On the other hand, if $V_r > V_c$ but the impact energy is not high enough to destroy the bodies, mass exchange occurs and the bodies will drift apart with new velocities that are a fraction of the initial impact velocity. The mass exchange process has two consequences: the loss of a small amount of mass and modification of the coefficient of restitution, i.e., the rebound velocity-impact ratio is reduced because there is a greater loss of energy in the impact. The modified coefficient of restitution is c_{ii} .

To account for this event, we need to calculate the mass loss and the velocity of the ejected debris. The ejected mass from m_1 after a mass-exchange impact by a body with mass m_2 with impact velocity V_r can be approximated by ([Greenberg et al. 1978](#)),

$$m_{\text{ej}}^{(1)} = c_{\text{ej}} K m_2 V_r^2 [V_e^{(1)}]^{-9/4}, \quad (6)$$

Here K is the mass excavation coefficient, c_{ej} is the ejecta velocity coefficient (both of which depend on intrinsic properties of the colliding bodies, see Table 2), and $V_e^{(1)}$ is the escape speed of the body with mass m_1 . In analogy, this analysis works for m_2 as well.

Considering mass exchange, the new masses are then,

$$\begin{aligned} m'_1 &= m_1 - m_{\text{ej}}^{(1)} + m_{\text{ej}}^{(2)}, \\ m'_2 &= m_2 - m_{\text{ej}}^{(2)} + m_{\text{ej}}^{(1)}. \end{aligned} \quad (7)$$

The new velocities can be derived to be,

$$\mathbf{v}'_1 = \mathbf{V}_G - \left(\frac{m_2}{M}\right) \mathbf{V}'_{\text{reb}}, \quad (8)$$

$$\mathbf{v}'_2 = \mathbf{V}_G + \left(\frac{m_1}{M}\right) \mathbf{V}'_{\text{reb}}.$$

¹ We are currently working on a self-consistent treatment of body densities, but for the time being such a model is beyond the scope of this work.

Table 2. Collision parameters (SI units) following [Alexander & Agnor \(1998\)](#).

Parameter	Symbol	Value	Units
Restitution coefficient	c_i	0.7	-
Modified restitution coefficient	c_{ii}	0.5	-
Maximum rebound velocity	V_c	55	m/s
Mass excavated coefficient	K	1.0×10^{-7}	$1/(\text{kg m}^2/\text{s}^2)$
Impact strength	S	3.0×10^7	J/m^3
Ejecta velocity coefficient	c_{ej}	3.0×10^6	m/s
Characteristic density	ρ_c	3×10^3	kg/m^3

3.1.3 Fragmentation

If the impact energy E is large enough, the internal structure of the body is destroyed. Fragmentation occurs when the energy per unit volume is greater than the impact strength, i.e. when $E > SW$, with W being the volume of the planet, the body will be shattered. After such a collision, fragments may coalesce again and new bodies may emerge.

The fragments of the destroyed body follow a power-law mass distribution ([Greenberg et al. 1978](#)), which yields fragments of which the largest has a mass m_{\max} that from experiments ([Fujiwara et al. 1977](#)) can be calculated to be,

$$m_{\max} = \frac{M}{2} \left(\frac{E}{SW} \right)^{-1.24}. \quad (9)$$

Here $M = m_1 + m_2$.

Following Section 3.1.2, the amount of mass leaving the two-body system is,

$$m_{ej} = c_{ej} M (V_e)^{-9/4}. \quad (10)$$

Here V_e is the escape speed for M . The remaining mass will coalesce into a new single body. For the mass distribution of the fragments escaping from the parent body a small number of bodies represented by four escaping bodies is assumed; it was chosen this way in order to prevent the number of particles from becoming too large. The mass of the new fragments is then,

$$\left. \begin{aligned} M_1 &= \frac{m_{ej} m_{\max}}{M}, \\ M_2 &= \frac{1}{\alpha} m_{\max}, \\ M_3 &= M_4 = \frac{3 - \alpha}{2\alpha} m_{\max}, \end{aligned} \right\} \alpha \geq 1 \quad (11)$$

$$M_1 = M_2 = M_3 = M_4 = \frac{m_{ej}}{4}, \quad \left. \right\} \alpha < 1. \quad (12)$$

Here $\alpha = 4m_{\max}/M$ is a proxy for the impact energy ($\alpha = 4m_{\max}/M = 2(E/SW)^{-1.24}$). Table 2 summarizes the numerical values chosen for the collision parameters.

3.2 Statistical framework

In order to make a global assessment of how a planetary system changes after considering its secular evolution, we built a statistical framework that allows us to directly compare how the planet architecture changes in a system. To do this, we non-parametrically estimate a probability distribution function for the planet eccentricities, masses, and semi-major axes for each system, before and after the planet orbits were allowed to evolve dynamically.

We estimate these distributions with the Kernel Density Estimation

(KDE) method. For a random sampling X_i of a given variable x , the KDE probability distribution function is,

$$p_{\text{KDE}}(x) = \frac{1}{nh} \sum_i K \left(\frac{x - X_i}{h} \right). \quad (13)$$

Here K is a smooth function called *kernel*, which we take to be Gaussian, and h is a parameter known as the bandwidth, which controls the amount of smoothing. We robustly estimate this parameter using a cross-validation method instead of the usual rules-of-thumb that are found in the literature.

The divergence, or statistical "distance" between two distributions is a measure of how much one distribution function differs from another. In this work we will use the Kullback-Leibler divergence [Kullback & Leibler \(1951\)](#), which is based on the Shannon information entropy, which in turn is inspired by the physical concept of entropy.

The relative entropy or the Kullback-Leibler distance between two probability functions $p(x)$ and $q(x)$ is thus defined as,

$$D(p||q) = \sum_i p(x_i) \log \frac{p(x_i)}{q(x_i)}. \quad (14)$$

Here $||$ indicates "divergence". The KL divergence estimates the number of additional bits (i.e., computed with the base 2 logarithm) needed to represent an event of a random variable. The better the approximation, the less additional information is required. If the divergence KL is zero it means that the two distributions are identical.

The Kullback-Leibler divergence (KL divergence hereafter) stands out among other statistical tests that measure the statistical distance between two distributions, such as the Kolmogorov-Smirnov test (KS) or the Cramer-von Mises criterion (CM), because it considers most of the domain of the distributions instead of focusing on point-estimates, thus giving equal weight to all the available data. The KL divergence is therefore sensitive to subtle differences near the tails of the distributions, which other frequentist tests tend to ignore.

Thus, we can use the KL divergence as an assessment of the change of the configuration of a planetary system before and after considering secular evolution for the selected variables: a significant change will yield a high KL divergence value and a small (or no) change will yield a KL divergence that is close to zero (see Figure 8 for an illustration). A systematic estimation of these changes across all synthetic systems from our Monte Carlo simulations will yield the parameter space of stellar parameters (e.g. stellar mass, metallicity) which will most likely result in a significant change in orbital configuration in terms of planetary mass, eccentricity, and semi-major axis.

4 RESULTS

In this work we want to address the question of the role of secular gravitational evolution in the final configuration of planetary systems. Our approach is based on a statistical assessment based on comparing the initial and final distribution of planets using the statistical framework described in Section 3.2. Additionally, we are interested in understanding how stellar parameters can have an influence in the dynamical evolution of the system.

We evolve synthetic planetary systems that are produced by a Monte Carlo planet population synthesis model (Section 2.2 considering gravitational interactions (and their consequences) with an N -body collisional simulator. To this end we numerically solve the equations of motion for a given planetary system using a Leapfrog

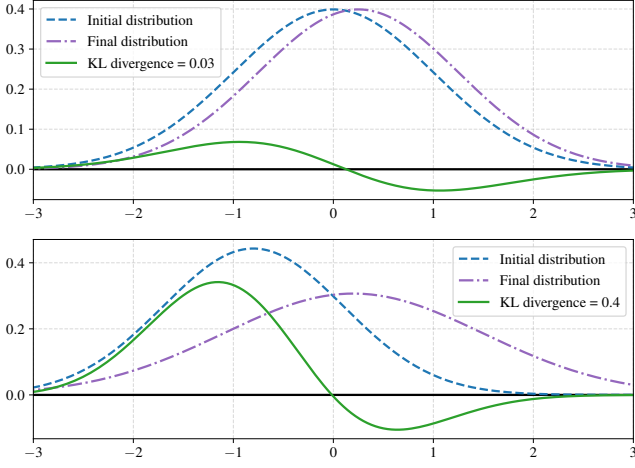


Figure 8. Illustrative plot showing how the Kullback-Leibler divergence works.

symplectic integrator. We chose this integrator because it ensures the energy conservation in large ($\sim 10^6$ yr) time scales. Additionally, we use the collisional recipe described in Section 3.1 in order to account for rebound, fragmentation, and mass transfer between planets.

We first ran a set of gravitational evolution simulations of a random sub-sample of 180 planetary systems over a period of 10^5 years, and then a different group of 192 systems over 10^6 years, adding up to a total ~ 4800 planets. The physical parameters from which planetary systems were synthesized according to the planet formation recipe used here are summarized in 1. The total computing time it took to run the simulations was ~ 64000 h, running at the ClusterCIEN cluster of the Institute of Physics of Universidad de Antioquia.

The final step in preparing the data for a statistical comparison was to reconstruct the distribution of planetary mass, semi-major axis and eccentricity using a cross-validated Gaussian KDE for the systems in their initial and in their final configuration (i.e. after gravitational evolution).

4.1 Secular evolution over 10^5 yr

Figure 9 shows a Gaussian KDE of the KL divergence between the before-and-after gravitational evolution of 180 planetary systems in terms of their planet mass, eccentricity and semi-major axis distributions. Most of the systems show a maximum a posteriori (MAP, e.g. the mode) of the KL divergence distribution near zero, which means that most systems experience little-to-no change after considering the effects of gravitational interactions after 10^5 yr. It also follows that the stability of a system on timescales up to 10^5 yr does not depend on stellar parameters.

However, the MAP of the KL divergence distribution of eccentricity is higher than the MAP for planet mass and semi-major axis. This shows that systems tend to change their eccentricity more than their mass and semi-major axis configurations. Indeed, almost all of the systems in our sample show a more significant change in their eccentricities than in their mass and semi-major axis configurations.

An inspection of the dependence of the eccentricity KL divergence on stellar parameters (Figure 10) shows that most systems uniformly change their eccentricity configurations regardless of the stellar mass and metallicity, as there is virtually no correlation with those stellar parameters. These changes seem to arise normally due

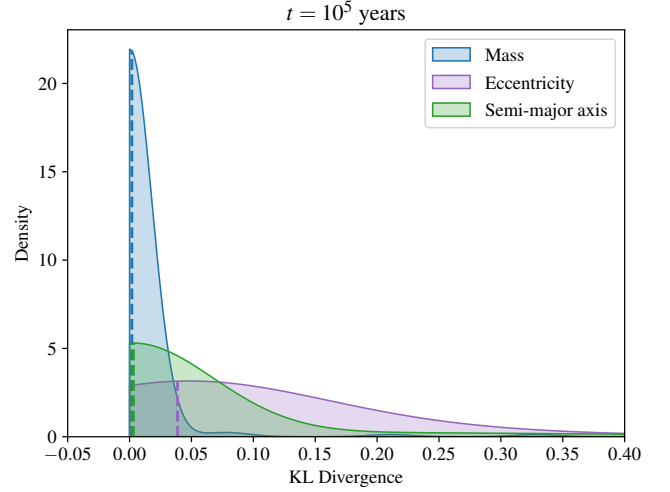


Figure 9. Gaussian KDE of the KL divergence between the mass, eccentricity and semi-major axis distributions of 180 planetary systems at $t = 10^5$ yr.

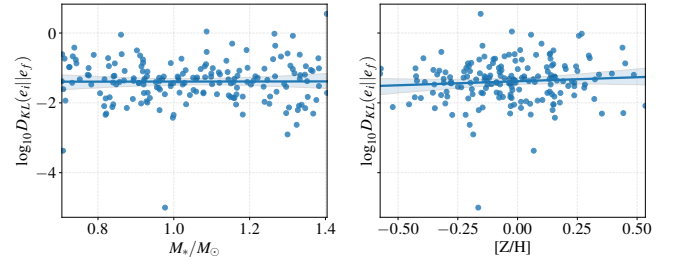


Figure 10. Linear regression of the KL divergence between the initial and final eccentricities vs. the mass and metallicity of the host star for 180 synthetic planetary systems at $t = 10^5$ yr.

to gravitational interactions without radically changing the overall orbital configuration.

Figure 9 also shows the presence of extended tails in the KL distributions for planet mass and semi-major axis. We identify the source of this feature as *outlier* systems, defined here as systems whose whose KL divergence is more than 1σ above the rest of the divergences from their sub-sample. Since one of our goals is to identify which factors may affect significant changes in the orbital configurations after evolution, we will discuss whether these outliers emerge randomly or from a specific set of physical conditions in Section 4.3. The fraction of outliers in terms of planet mass and semi-major axis KL divergence is shown in Table 3.

4.2 Secular evolution over 10^6 yr

In order to achieve a realistic timescale for when a final configuration of a planetary system emerges, we took a sub-sample of 192 synthetic planetary systems and ran our gravitational collisional N -body simulations for 10^6 yr. Figure 11 shows a Gaussian KDE of the KL divergence between the initial and final configuration of planetary systems in terms of their orbital parameters. Similar to the 10^5 yr evolution case described in the previous section, the MAP of the KL divergence distributions for mass and semi-major axis are near zero, with a higher MAP of the KL divergence for eccentricity. Again, this means that a) most of the systems do not show a change in their planet mass and eccentricity configurations, whereas many systems change

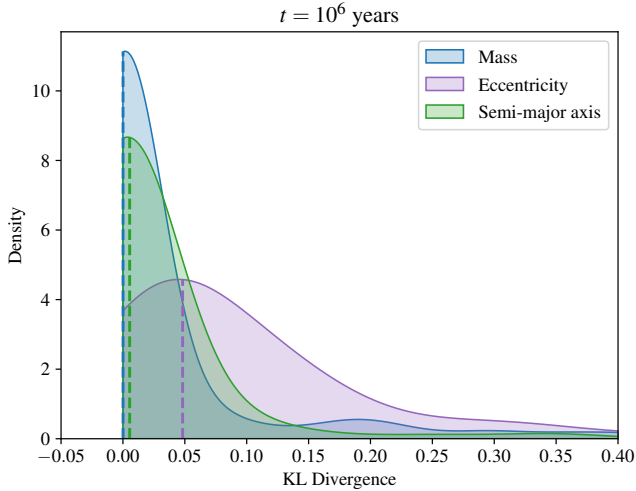


Figure 11. Gaussian KDE of the KL divergence between the mass, eccentricity and semi-major axis distributions of 180 planetary systems at $t = 10^6$ yr.

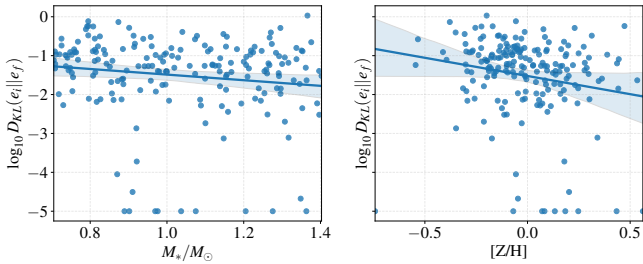


Figure 12. Linear regression of the KL divergence between the initial and final eccentricities vs. the mass and metallicity of the host star for 180 synthetic planetary systems at $t = 10^6$ yr.

their eccentricities after 10^6 yr of gravitational interactions, and b) that the stability of most systems for up to 10^6 yr is not dependent on stellar parameters.

Figures 9 and 11 show that more systems evolving for 1 Myr change their orbital configuration when compared to systems evolving for only 100 kyr. Indeed, the fraction of systems that show a significant change in their planet mass and semi-major axis configurations in Table 3 shows this. Still, note that the fraction of systems that change their orbital configuration remains small.

Figure 12 shows the eccentricity KL divergence vs. stellar parameters. Although there seems to be a negative correlation, the confidence bands in a linear regression show that this correlation is very weak (i.e. a slope = 0 model fits within the bands). Since there seem to be no particular outliers (other than at the low KL-divergence end) for either of the time periods considered in this work, we can conclude that even though planetary eccentricities are sensitive to gravitational interactions, they do not radically alter the overall planet mass or semi-major axis configurations.

4.3 Outlier systems

We now turn to a discussion on whether systems that experience changes in orbital configuration (outliers) as shown by an above 1σ deviation in their KL divergence appear at random or if they are more likely to appear in systems with specific ranges of stellar parameters.

Table 3. Percentage of outliers (i.e. systems changing their orbital configuration after gravitational evolution) based on the KL divergences between masses and semi-major axis distributions for 10^5 and 10^6 years of evolution.

	KL Divergence of:	
	Mass (M_{\oplus})	Semi-major axis (AU)
% in sim: 10^5 years	2.77	10.00
% in sim: 10^6 years	11.45	5.72

Table 4. Range of stellar masses and metallicities in which planetary mass outliers and semi-major axis outliers were found. The number of outliers compared to the total number of systems within the same stellar mass and metallicity range is reported below each value.

Simulation group: 10^5 years		
Mass	$M_{\odot} = 1.27^{+0.05}_{-0.05}$	$[Z/H] = 0.27^{+0.11}_{-0.12}$
	5/23 systems	5/29 systems
Semi-major axis	$M_{\odot} = 1.14^{+0.18}_{-0.29}$	$[Z/H] = 0.15^{+0.21}_{-0.16}$
	18/124 systems	18/70 systems
Simulation group: 10^6 years		
Mass	$M_{\odot} = 1.08^{+0.19}_{-0.19}$	$[Z/H] = 0.03^{+0.27}_{-0.14}$
	22/97 systems	22/117 systems
Semi-major axis	$M_{\odot} = 1.07^{+0.26}_{-0.17}$	$[Z/H] = -0.06^{+0.37}_{-0.11}$
	11/112 systems	11/136 systems

Table 3 shows that less than 10% of systems experience this change, i.e. about 40 systems.

We can therefore retrieve plausible correlations between stellar parameters and the likelihood that a planetary system will experience significant changes in its final orbital configuration. Given that most (90%) of the systems in our sample do not experience such a change, i.e. their KL divergence remains near zero after gravitational evolution, we are interested in the few outlier systems that do experience changes in their orbital configuration, informed by the KL divergence. Recall that since we calculate different KL divergences for planet mass and semi-major axis distributions, there are *mass* outliers and *semi-major axis* outliers.

Figures 13 and 14 show a comparison between stellar masses and metallicities of outlier systems and the whole sub-sample of systems evolving to 10^5 and 10^6 yr, respectively. From this comparison we can see that systems with higher stellar masses are more likely to change their orbital configuration in terms of planet mass and semi-major axis. This is likely due to the host star having a more significant gravitational influence over the orbital configuration of planets, whose initial locations are set by the local protoplanetary disk conditions and the result of migration processes and not from any secular relaxation.

In particular, for systems evolving to 10^5 yr, significant planetary mass changes occurred in 22% of the systems with stellar masses in the range $1.22M_{\odot} < M_{\star} < 1.32M_{\odot}$ and 17% of the systems with metallicities between 0.15 and 0.38. Changes in semi-major axis occurred for 15% of the systems with stellar masses in the range $0.85M_{\odot} < M_{\star} < 1.32M_{\odot}$ and 26% of the systems with metallicities between -0.01 and 0.36 .

Similarly, for systems evolving to 10^6 yr, planetary mass changes happened for 23% of the systems with stellar masses in the range $0.89M_{\odot} < M_{\star} < 1.27M_{\odot}$ and 19% of the systems with

metallicities between -0.11 and 0.3 . Changes in semi-major axis occurred for 10% of the systems with stellar masses in the range $0.9M_{\odot} < M_{\star} < 1.33M_{\odot}$ and for 8% of the systems with metallicities between -0.17 and 0.31 . This is summarized in Table 4.

Similarly, the 10^5 yr sub-sample shows that systems whose stars are metal-rich are more likely to change their orbital configuration in terms of mass and semi-major axis. This is likely due to the fact that metal-rich disks form more massive cores which in turn leads to a higher rate of giant planet formation. Giant planets are expected to be uncommon according to most planetary synthesis simulations, but they can significantly impact the orbital configuration of the planetary system which they inhabit.

This correlation of outliers with metallicity for our sub-sample evolving to 1 Myr seems to hold inasmuch outlier systems tend to have metallicities slightly higher than Solar. However, this is not as clear-cut as in the previous case (10^5 yr) since the original sub-sample is also slightly skewed toward higher metallicities.

To summarize, the range of stellar parameters for outliers (Table 4) show a narrow, skewed range relative to the full range of the simulations shown in Table 1, further evidenced in the comparison between distributions in Figures 13 and 14. This means that outliers do not appear as statistical flukes, but rather seem to come from an underlying distribution which may help evince a plausible physical explanation for orbital alteration.

We should note that as per our population synthesis simulations only 1 in 5 systems have giant planets, and therefore most of the dynamical simulations are performed with systems with lighter planets where orbital disruption is less likely. Further simulations with a larger sample of systems may be able to clear this up, but this lies outside of the exploratory scope of this work.

4.4 Host stars of outliers vs. observations

Although our results above show that secular gravitational interactions seldom alter the final orbital configuration of a planetary system, outlier systems (i.e., systems that do change configuration) share enough commonalities that an inspection of their stellar parameters can inform us of the conditions in which an orbital configuration change is more likely. In this section we explore the plausibility of observed systems having had a late, dynamic orbital evolution, by comparing the stellar parameters of outlier systems and those of the whole *exoplanets.eu* sample of observed exoplanetary systems.

Figure 15 shows a comparison of the normalized mass distribution and stellar metallicity of *exoplanets.eu* systems vs. outliers. We make this direct comparison between differently biased system populations to point out that the range of stellar parameters where outliers may occur falls within the range of stellar parameters of observed systems, therefore showing that outliers do not form in unphysical or otherwise extremely pathological conditions.

Notice that the histogram density is proportional to the number of synthetic systems whose orbital configuration changed for a given range of stellar mass or metallicity. It is evident that outlier systems have stellar parameters within the range of observations, showing that it is plausible (although still unlikely) that some observed planetary systems have experienced significant orbital changes. In particular, it is unlikely that observed systems with host stars of spectral types K-M experienced a significant orbital change; a change in orbital configuration is more likely in systems around G- and F-type stars.

Similarly, no outlier systems are found for metallicities much lower than solar: outliers can be found for host stars with metallicities above -0.2 with the probability peaking at $0.1 - 0.2$. Therefore, massive stars composed of more heavy elements (compared to Solar) are more

likely to have planetary systems that have experienced substantial orbital changes during the dynamical evolution of planetary systems.

We should emphasize that differences in the observed and simulated populations as illustrated here may be due to observational biases affecting the distribution of the observed population, and thus observations of massive and metal-rich stars may not necessarily be more likely to reveal signs of center-of-mass changes at the late stages of planet formation identified by our simulations.

4.5 Planetary system reclassification after gravitational evolution

We end this discussion of results with an analysis inspired by our center-of-mass classification scheme from Section 2.3. In our method described above, we use the posterior distributions from the GMM clustering scheme in order to check whether a system is reclassified after considering the center-of-mass uncertainty. Here we borrow the basics from this analysis in order to check whether a system is reclassified after its secular evolution. We should clarify that reclassification due to dynamical evolution and reclassification due to measurement errors cannot be directly compared, as the former refers to the same synthetic system evolving and possibly changing during a time span of more than 10^5 yr and the latter refers to whether we know enough about an observed system to properly classify it in terms of its r_{cm} .

As expected from our results (summarized in the previous section), for most cases the center of mass r_{cm} of the evolved system is still close to its original value and therefore they are not reclassified. However, for outlier systems the semi-major axis and planetary mass distributions change and therefore their center of mass also changes, leading to a reclassification. We shall take a look at the results from this analysis, with *planet mass outliers* meaning systems whose planet mass configuration changed, and *semi-major axis outliers* meaning systems that experienced changes in their semi-major axis configurations after secular evolution.

- *Outliers in systems evolving to 10^5 yr.* 33% of the semi-major axis outliers and 20% of the planet mass outliers are reclassified to *Sub-Mercurian* from other clusters (see the original clustering of synthetic systems in Figure 7). Thus, outliers produce a down-shift in the center of mass r_{cm} towards the $0.2 - 1$ AU region. We also noticed that planet mass outliers often occur in systems that lose planets in gravitational interactions with massive planets.

- *Outliers in systems evolving to 10^6 yr.* 54% of semi-major axis outliers are reclassified, but not to any particular cluster. 40% of planet mass outliers are reclassified, most of them as *Sub-Mercurian*. To wit, when there is a loss of a planet (or more), the center of mass decreases, whereas a shift in the semi-major axis configuration may not necessarily lead to planet loss, so the center of mass shift can be in any direction.

5 CONCLUSIONS

In this work we are interested in finding the conditions which set apart planetary systems that significantly change their planet mass and semi-major axis configurations after allowing for dynamical evolution. To this end, we evolve ~ 400 synthetic planetary systems with ~ 5000 planets forward in time using an adaptive-step collisional N-body simulator. Our seed planetary systems were created from a Monte Carlo planet population synthesis model, using the star-disk distributions in Table 1 as initial conditions.

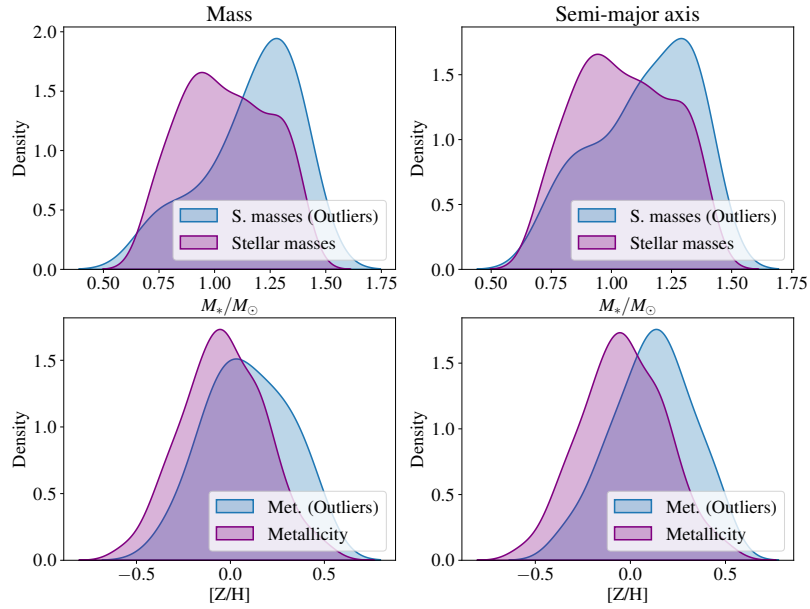


Figure 13. Stellar mass and metallicity distributions of the mass and semi-major axis outlier systems in the sim group: 10^5 years.

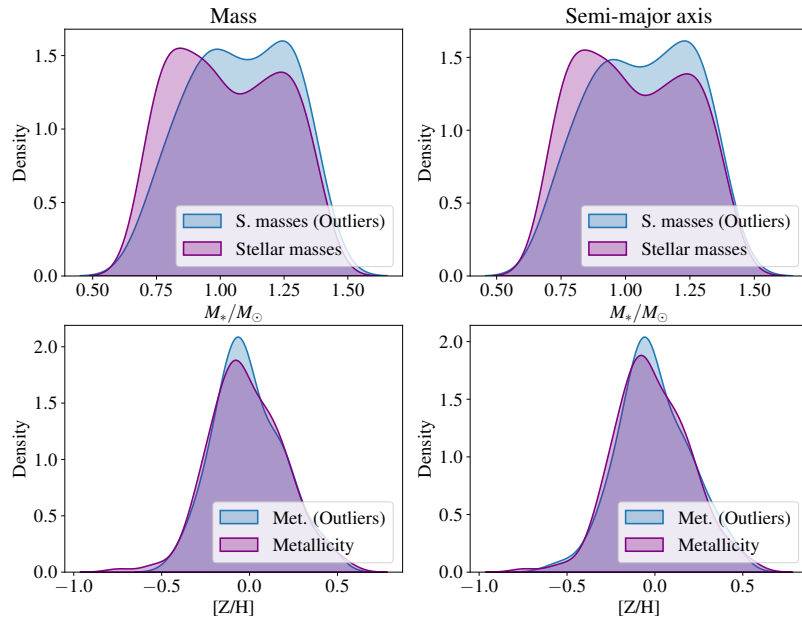


Figure 14. Stellar mass and metallicity distributions of the mass and semi-major axis outlier systems in the sim group: 10^6 years.

In order to better understand the architecture of observed and synthetic planetary systems and how it may change we first built a clustering scheme for the center of mass r_{cm} (as defined in Section 2.3) based on Gaussian Mixture Models and Information Criteria. In the case of observed planetary systems we included an additional model validation step based on Approximate Bayesian Computation methods.

Our methods yielded four groups of observed planetary systems: *Sub-Mercurian* for $10^{-2} \text{ AU} \leq r_{\text{cm}} < 10^{-1} \text{ AU}$ with 46.0% of observed systems, *Venusian* for $10^{-1} \text{ AU} \leq r_{\text{cm}} < 1 \text{ AU}$ with 12.8% of observed systems, *Solar-like* for $1 \text{ AU} \leq r_{\text{cm}} < 10 \text{ AU}$ with 37.0% of observed systems, and *Peripheral* for $10 \text{ AU} \leq r_{\text{cm}}$ with

4.20% of observed systems. Our Approximate Bayesian Computation validation method found that our scheme is robust, with less than 2% of systems being re-classified when taking measurement errors into account.

We found that synthetic planetary systems are also best classified by 4 clusters of r_{cm} , corresponding to the same clusters found for the observed systems (within a factor 2), albeit with radically different posterior amplitudes that are due to observational biases.

In order to assess the possible change of orbital configuration in a system after gravitational evolution we used a statistical framework based on a cross-validated Kernel Density Estimation of the planet mass, semi-major axis, and eccentricity and a calculation of

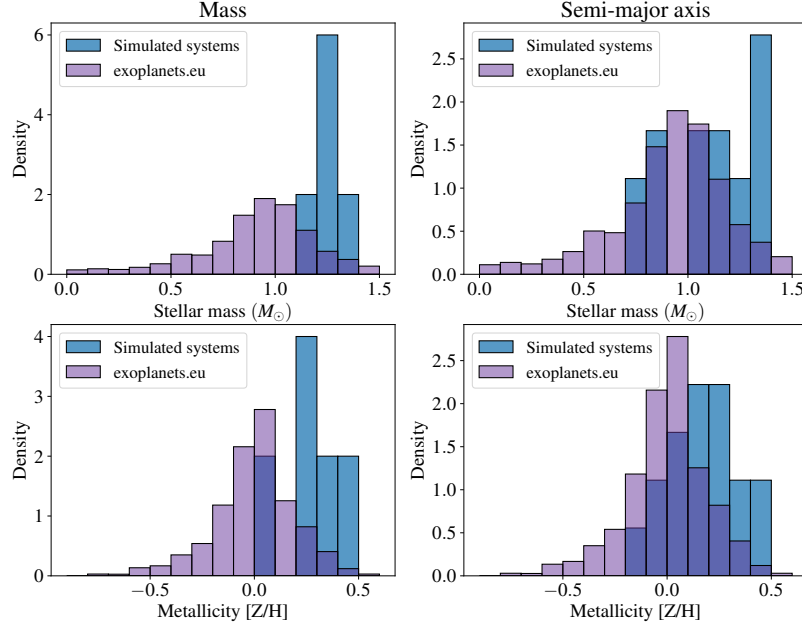
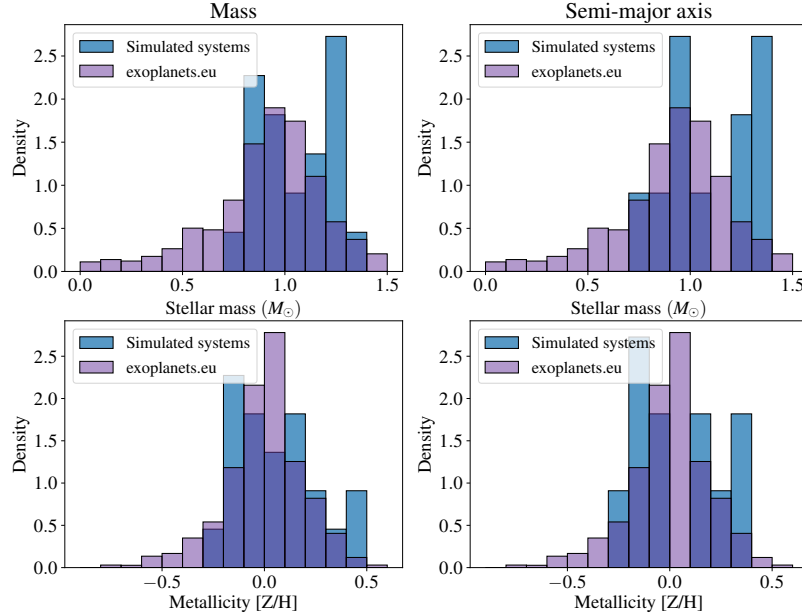

 (a) Systems evolving to 10^5 yr.

 (b) Systems evolving to 10^6 yr.

Figure 15. Stellar mass and metallicity distribution of outlier systems in the *exoplanets.eu* database and simulated systems.

the Kullback-Leibler divergence between the before-and-after distributions as a Bayesian measurement of the statistical distance between the initial and final orbital configurations.

After letting the synthetic systems evolve gravitationally to 10^5 and 10^6 yr we found that $\geq 90\%$ of the systems present a stable dynamical evolution, that is, their orbital parameters (planet mass, eccentricity, semi-major axis) do not significantly change during the latter stages of planetary formation.

However a few systems ($\leq 10\%$) had statistically significant changes, which we refer to in the text as *outliers*: planetary systems whose KL divergence is above 1σ above the mean. Further analysis of these outliers shows that even though they may appear

at almost any realistic stellar mass or metallicity, systems with F- and G- type host stars are much more likely to experience changes in their orbital configuration when compared to systems with K- and M- type host stars. This is compatible with the Nice Model [Tsiganis et al. \(2005\)](#), which suggests a scenario for the young Solar System in which its original orbital configuration changed due to gravitational interactions with leftover planetesimals. Likewise, systems with metallicities higher than solar ($[\text{Fe}/\text{H}] > 0.2$) are also more likely to change their orbital configuration due to interactions with massive planets. This is mostly due to the fact that giant planets are more likely to be found in systems with high stellar metallicity.

We noticed differences between the distribution of outliers vs. the

rest of synthetic systems and vs. observed systems. On one hand, the former is significant because it tells us that the specific mass and metallicity conditions shown here favor orbital configuration changes. On the other hand, the latter may be due to observational biases, which means that further observations of already discovered massive, metal-rich stars may not be as informative as discovering new planet-hosting stars.

Finally, we check whether outliers are reclassified in our clustering scheme after dynamical evolution. Interestingly, only about 20-50% outliers (less than 10 systems out of nearly 400 total) are reclassified, meaning that statistically significant changes in r_{cm} do not necessarily translate to significant changes in cluster membership. Our classification scheme is thus proven to be fairly robust with respect to observational uncertainties and gravitational evolution effects.

Since outliers are usually classified as Sub-Mercurian in terms of their center of mass, we conclude that orbital configuration changes are related to the presence of massive, migrated planets. These close-in giants alter the orbital stability of newly born planetary systems, in many cases causing scenarios where other planets are ejected from the system.

In future work we will focus on running more simulations from our original pool of synthetic systems (and for longer timescales). Thus we will more thoroughly sweep the parameter space to better quantify the precise causes behind changes in orbital configurations brought about by secular gravitational interactions.

ACKNOWLEDGEMENTS

The authors would like to thank: Yamila Miguel for providing the first version of the Planet Population Synthesis code, Jaime Forero-Romero for giving us access to the UniAndes computing facilities in which this code was run to produce our synthetic planetary system dataset, Pablo Cuartas and Mateo Restrepo for providing us with the first version of the N-body collisional simulation code, Santiago Vargas and Mario Acero for their valuable feedback. We would also like to thank the anonymous referee for their insight, which helped convey our conclusions more clearly.

DATA AVAILABILITY

Initial data from the simulations can be found at: https://github.com/saint-germain/population_synthesis/tree/master/data_from_sim. The rest of the data and code are available upon request.

REFERENCES

- Akaike H., 1974, *IEEE Transactions on Automatic Control*, 19, 716
- Alexander S., Agnor C., 1998, *Icarus*, 132, 113
- Alibert Y., Mordasini C., Benz W., 2011, *Astron. Astrophys.*, 526, A63
- Alvarado-Montes J. A., Zuluaga J. I., Sucerquia M., 2017, *Monthly Notices of the Royal Astronomical Society*, 471, 3019
- Andryushin A. S., Popov S. B., 2021, *Astron. Rep.*, 65, 246
- Armitage P. J., 2018, *Handbook of Exoplanets*, p. 2185–2203
- Bashi D., Zucker S., 2021, *Monthly Notices of the Royal Astronomical Society*, 510, 3449
- Bashi D., Helled R., Zucker S., 2018, *Geosciences*, 8, 325
- Beaugé C., Aarseth S., 1990, *Monthly Notices of the Royal Astronomical Society*, 245, 30
- Benz W., Ida S., Alibert Y., Lin D., Mordasini C., 2014, in *Protostars and Planets VI*. p. 691, doi:10.2458/azu_uapress_9780816531240-ch030
- Bryson S., et al., 2021, *AJ*, 161, 36
- Chaparro Molano G., Bautista F., Miguel Y., 2018, *Proceedings of the International Astronomical Union*, 14, 152–155
- Claeskens G., Hjort N. L., 2008, *Model Selection and Model Averaging*. Cambridge Series in Statistical and Probabilistic Mathematics, Cambridge University Press, doi:10.1017/CBO9780511790485
- Exoplanet Exploration Program, NASA 2010, Exoplanet Exploration Program, NASA’s search for habitable planets and life beyond our solar system, Url/https://exoplanets.nasa.gov/exep/
- Fujiwara A., Kamimoto G., Tsukamoto A., 1977, *Icarus*, 31, 277
- Greenberg R., Wacker J. F., Hartmann W. K., Chapman C. R., 1978, *Icarus*, 35, 1
- Guerrero N. M., et al., 2021, *ApJS*, 254, 39
- Ida S., Lin D. N. C., 2004, *The Astrophysical Journal*, 604, 388
- Kipping D. M., Sandford E., 2016, *Mon. Not. Roy. Astron. Soc.*, 463, 1323
- Kullback S., Leibler R. A., 1951, *The annals of mathematical statistics*, 22, 79
- Liu B., Raymond S. N., Jacobson S. A., 2022, *Nature*, 604, 643
- Miguel Y., Guilera O. M., Brunini A., 2011, *Mon. Not. Roy. Astron. Soc.*, 417, 314
- Mordasini C., Alibert Y., Benz W., 2009a, *Astron. Astrophys.*, 501, 1139
- Mordasini C., Alibert Y., Benz W., Naef D., 2009b, *Astron. Astrophys.*, 501, 1161
- Naderi M., Hung W. L., Lin T. I., Jamalizadeh A., 2019, *J. Multivar. Anal.*, 171, 126
- Pedregosa F., et al., 2011, *Journal of Machine Learning Research*, 12, 2825
- Raymond S. N., O’Brien D. P., Morbidelli A., Kaib N. A., 2009, *Icarus*, 203, 644
- Rogers J. G., Owen J. E., 2021, *MNRAS*, 503, 1526
- Schlecker, M. et al., 2021, *A&A*, 656, A73
- Schneider J., Dedieu C., Sidaner P. L., Savalle R., Zolotukhin I., 2011, *Astron. Astrophys.*, 532, A79
- Schwarz G., 1978, *Ann. Statist.*, 6, 461
- Sucerquia M., Ramírez V., Alvarado-Montes J. A., Zuluaga J. I., 2019, *Monthly Notices of the Royal Astronomical Society*, 492, 3499
- The Extrasolar Planets Encyclopaedia 1995, The Extrasolar Planets Encyclopaedia Kernel Description, <http://exoplanet.eu/>
- Tsiganis K., Gomes R., Morbidelli A., Levison H. F., 2005, *Nature*, 435, 459
- Udry S., Santos N. C., 2007, *Annu. Rev. Astron. Astrophys.*, 45, 397
- VanderPlas J., 2016, *Python Data Science Handbook: Essential Tools for Working with Data*, 1st edn. O’Reilly Media, Inc.
- Woo J., Brasser R., Grimm S., Timpe M., Stadel J., 2022, *Icarus*, 371, 114692

This paper has been typeset from a $\text{\TeX}/\text{\LaTeX}$ file prepared by the author.